Development of a Microstructure Prediction Model for Aeroengine Metallic Materials

URATANI Masato : Material Processing Technology Department, Production Engineering Center, Corporate Research & Development
SAITO Minako : Material Processing Technology Department, Production Engineering Center, Corporate Research & Development
NISHII Takashi : Manager, Material Processing Technology Department, Production Engineering Center, Corporate Research & Development

Aeroengine parts are produced by carrying out casting, powder metallurgy, and plastic forming techniques such as forging. Forged products usually have little variation in terms of strength so this method is applied when a high degree of reliability is needed. In addition to the product's dimensions and strength, requirements are also set with regard to the quality of the microstructure if a particularly high degree of reliability is required. Based on these requirements, IHI is developing a new microstructure prediction model that takes into consideration the physical mechanism that occurs during the forming process in order to accurately simulate the microstructure evolution. This paper discusses crystal-plasticity finite element method (CPFEM) simulations, which form part of the new model.

1. Introduction

Aeroengines are products that must be of high quality, and plastic working is applied in a portion of the manufacturing process of their metal parts. For forged parts, which must have particularly high reliability, quality requirements for microstructures are set in addition to the conventional dimensional requirements. Crystal grain size is a typical example of microstructure requirements; microstructure control must be performed so that the crystal grain size is within a prescribed range. In recent years, near-net-shape forging (a manufacturing technique to form each product close to the final shape by forging) has increasingly been applied. Accordingly, process design techniques for highly accurate control of both the shape and microstructure are required.

In the development of manufacturing processes that use metal forming, simulation is essential to shorten the development period and to reduce costs. Prediction of part shapes formed by plastic working has increasingly been made more accurate in practice by applying deformation analysis based on the Finite Element Method (FEM), mainly using a general-purpose solver. By contrast, microstructure evolutions have conventionally been predicted by using empirical formulae based on parameter fitting. However, for various reasons, this approach is not sufficiently practical. For example, it can neither deal with a wide range of forging conditions nor take into account the influence of deformation history. As a result, verification through trial manufacture is always necessary in the process development stage.

One factor that renders microstructure prediction difficult is the complexity of microstructure evolutions during deformation. For example, a compressor blade parts undergo a manufacturing process that applies hot forging, which consists of steps such as material heating, forging, cooling and heat treatment. During this manufacturing process, phenomena such as recovery, recrystallization and grain growth occur, and the state of microstructure change by the moment in response to the amount of strain, strain rate, and temperature. It is no easy task to represent these phenomena accurately by empirical formulae.

Along with recent developments in computers, new techniques for microstructure prediction are drawing attention. Those techniques are based on physically meaningful approaches in which physical phenomena occurring in the processes of microstructure evolutions are represented by theoretical formulae. One such technique is crystal plasticity simulation, which is performed by taking into account the physical mechanisms of plastic deformation in metal materials e.g. slip deformation. Crystal plasticity simulation is expected to enable prediction of the strain distribution and changes in crystal orientation that occur at the microscopic crystal grain level during macroscopic deformation, without applying any special assumptions according to the forging conditions. The amount of strain and the change in crystal orientation affect microstructure evolutions, such as recrystallization and grain growth[(1)]. Thus, it is important to first prediction factors in such microstructure evolutions.

We conducted fundamental examinations by focusing on the cold uniaxial compression deformation of Alloy718, a material for aeroengines. This paper describes the results and our discussions through the comparison and verification that we performed on the results of crystal plasticity simulation and experimental results.

2. Simulation method

2.1 Overview of crystal plasticity FEM

This section gives a brief overview of crystal plasticity FEM. For the details of the crystal plasticity simulation, refer to Reference (2).

Slip deformation is a basic mechanism of the plastic deformation in metal materials. For example, Alloy718 has a Face Centered Cubic (FCC) structure. **Figure 1** shows typical slip systems of FCC metal. The combination of the plane and the direction illustrated in the figure is referred to as a slip system. It is known that plastic deformation occurs when atoms move along a slip system. In crystal plasticity FEM, this microscopic deformation is expressed as the slip rate $\dot{\gamma}^{(\alpha)}$, and only the slip system α, in which the resolved shear stress $\tau^{(\alpha)}$ (the component in the direction of the slip system of macroscopic stress σ) becomes larger than the slip resistance $g^{(\alpha)}$, contributes to plastic deformation. These values are given by the following Equations (1) and (2)[3].

$$\dot{\gamma}^{(\alpha)} = \dot{\gamma}_0 \left| \frac{\tau^{(\alpha)}}{g^{(\alpha)}} \right|^{\frac{1}{m}} \mathrm{sign}\left(\tau^{(\alpha)}\right) \quad \cdots\cdots(1)$$

$$\tau^{(\alpha)} = \boldsymbol{\sigma} : \left(\boldsymbol{s}^{(\alpha)} \otimes \boldsymbol{m}^{(\alpha)}\right) \quad \cdots\cdots(2)$$

$\dot{\gamma}_0$: Reference slip rate
m : Strain rate sensitivity exponent (constant ranging from 0.001 to 0.002)
$\boldsymbol{s}^{(\alpha)}$: Slip direction vector
$\boldsymbol{m}^{(\alpha)}$: Slip plane normal vector

According to Equation (1), when m = 0.020, for example, the exponent becomes a large value of $1/m$ = 50. When $\tau^{(\alpha)} > g^{(\alpha)}$, $|\dot{\gamma}^{(\alpha)}| > 0$ holds; therefore, slip deformation occurs. This crystal level slip is associated with the plasticity part of the velocity gradient tensor that characterizes the macroscopic deformation rate, which is thus incorporated into the theoretical formulae for FEM.

Once plastic deformation occurs, various changes occur in the microstructures of metal material. Work hardening (a phenomenon in which materials harden due to plastic deformation) is a typical example of such a change. Various equations have been proposed as model formulae for expressing work hardening; this paper adopts Equations (3) and (4)[4] because these equations have been applied to aluminum alloys with the same FCC structure as Alloy718.

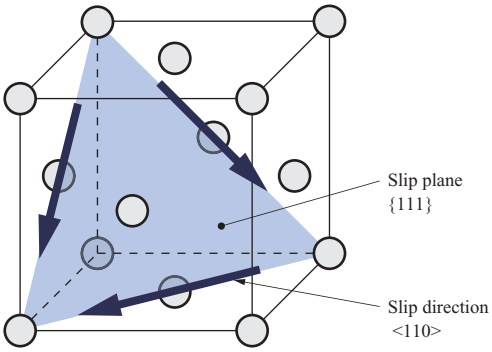

(Notes) (1) Slip systems depend on crystal structures. In a face centered cubic structure, the slip plane is {111}, and the slip direction is <110>.
(2) The illustrated portion is part of the structure. There are a total of 12 combinations of an equivalent plane and direction.

Fig. 1 Slip systems in the FCC metal

$$\dot{g}^{(\alpha)} = \sum_{\beta=1}^{N} h_{\alpha\beta} \left| \dot{\gamma}^{(\beta)} \right| \quad \cdots\cdots(3)$$

$$h_{\alpha\beta} = q_{\alpha\beta} \frac{\mathrm{d}\tau(\gamma)}{\mathrm{d}\gamma} + \left(1 - q_{\alpha\beta}\right) \frac{\mathrm{d}\tau(\gamma)}{\mathrm{d}\gamma} \delta_{\alpha\beta} \quad , \quad \frac{\mathrm{d}\tau(\gamma)}{\mathrm{d}\gamma} = h_0 \mathrm{sech}^2 \frac{h_0 \gamma}{\tau_s - \tau_0} \quad \cdots\cdots(4)$$

N : Number of slip systems
γ : Accumulated shear strain
$q_{\alpha\beta}$: Interaction matrix
h_0 : Initial hardening coefficient
τ_0 : Critical resolved shear stress
τ_s : Saturated resolved shear stress
$\delta_{\alpha\beta}$: Kronecker delta

In Equation (4), $h_{\alpha\beta}$ always takes a positive value. This fact means that when a microscopic slip occurs, the slip resistance becomes large.

In addition, the crystal orientation rotates in accordance with macroscopic deformation moment by moment. These changes are expressed by giving rotation to the slip direction vector and the slip plane normal vector through an elastic spin tensor $\boldsymbol{W}^{\mathrm{e}}$ as shown in Equation (5).

$$\dot{\boldsymbol{s}}^{(\alpha)} = \boldsymbol{W}^{\mathrm{e}} \boldsymbol{s}^{(\alpha)}, \qquad \dot{\boldsymbol{m}}^{(\alpha)} = \boldsymbol{W}^{\mathrm{e}} \boldsymbol{m}^{(\alpha)} \quad \cdots\cdots(5)$$

Above, we gave an overview of crystal plasticity FEM. Each constitutive equation has been expanded into various forms by different researchers, and many more complex and advanced equations have been proposed. The aforementioned constitutive equations are relatively simple and easy to use. Thus, in this paper, those equations are used at this stage.

2.2 Procedure for simulation by crystal plasticity FEM

(1) Finite element model

When crystal plasticity calculation is applied to a model of the entire workpiece, enormous amounts of calculation time is required. Therefore, we extracted a representative region of the workpiece's inside as the evaluation target, and we modeled it into a cube (side length: approximately 30 μm) containing multiple crystal grains. **Figure 2** shows the strain distribution in the workpiece that was subjected to uniaxial compression and the measurement points in Electron Backscatter Diffraction (EBSD). The forming simulation of the entire workpiece was performed in advance by rigid plasticity FEM, and three regions (the ① center part, ② side part and ③ upper part) that differed distinctly in the strain state after deformation as illustrated in **Fig. 2** were selected as the evaluation targets. The equivalent strains in the simulation results were approximately 0.8, 0.5 and 0.2, respectively. **Figure 3** shows the created finite element model. Grain

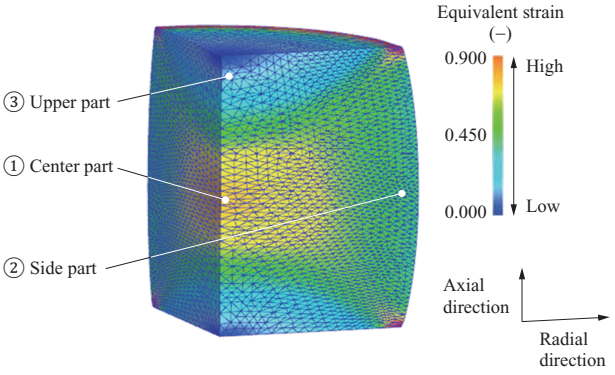

(Note) Axisymmetric1/4 model

Fig. 2 Strain distribution in a workpiece subjected to uniaxial compression and three observation points in EBSD

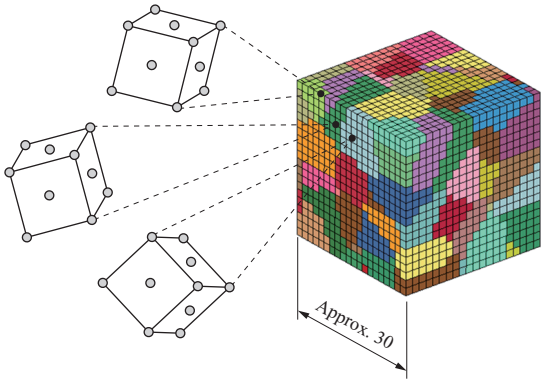

(Notes) (1) Each crystal grain is color-coded.
(2) Each crystal grain has a different crystal orientation.
(3) The orientations of the FCC crystal lattices illustrated to the left indicate their orientations.

Fig. 3 Finite element model used in the CP-FEM (unit : μm)

boundaries were generated by applying Voronoi division (a method for dividing a space containing a large number of points into small divisions from the perspective of which point is closest to each division)[5] as illustrated in the figure. Thus, the size and shape of a single crystal grain were expressed as multiple solid hexahedra elements. The number of elements was set to 8 000, and the number of crystal grains was set to 100. Each crystal grain was given the initial crystal orientation based on the experimental data obtained by EBSD measurement before deformation.

(2) Identification of material parameters

To accurately reproduce stress changes due to deformation, it is necessary to identify the material parameters that determine the relationship between stress and strain. **Figure 4** shows the results of parameter identification. We performed a uniaxial tensile test on an Alloy718 bar to determine the values of h_0, τ_0 and τ_s in Equation (4) so that the relationship between stress and strain in crystal plasticity FEM would agree with the test results.

(3) Setting of boundary conditions

To represent the strain state, which differs among selected microscopic regions, boundary conditions were

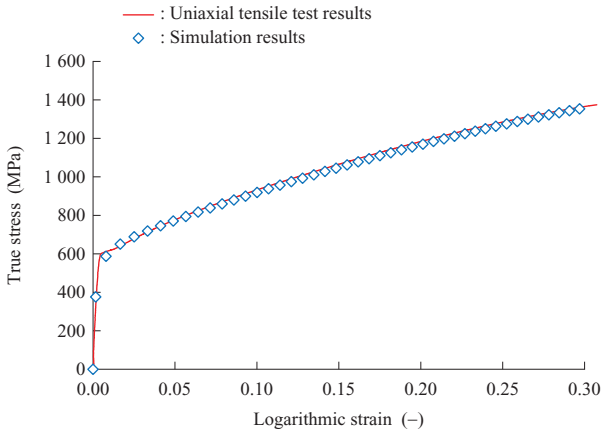

(Note) m (stain rate sensitivity exponent) : 0.020
$\dot{\gamma}_0$ (reference slip rate) : 0.033
τ_0 (critical resolved shear stress) : 190 MPa
τ_s (saturated resolved shear stress) : 470 MPa
h_0 (initial hardening coefficient) : 300

Fig. 4 Stress-strain curves obtained in the uniaxial tension test conducted in the experiment and the CP-FEM

set as follows.

① Displacement history data at the evaluation areas were obtained by ordinary rigid plasticity FEM.

② The displacement history was applied as boundary conditions to the six surfaces of the simulation model in crystal plasticity FEM.

Thus, each evaluation area was given a finite element model and boundary conditions, and calculations were performed separately for each area.

(4) Implementation of simulation

We independently developed crystal plasticity program code by using a user subroutine function of general-purpose FEM software. In this paper, calculations were performed with this program code.

3. Experimental method

To obtain data to evaluate the adequacy of the simulation results, we performed a cold uniaxial compression test on Alloy718. A press machine was used to apply deformation of a compression ratio (height after deformation / initial height) of 40% at an average strain rate of approximately 0.5 s^{-1} to a cylindrical workpiece with a diameter of 19 mm and a height of 28 mm.

To examine the microstructure evolutions, we cut the workpiece along its center cross section and polished it before and after deformation. We then performed EBSD measurement to observe the microstructure at the three evaluation areas shown in **Fig. 2**.

4. Results and discussions

4.1 Cold uniaxial compression test

This section will first describe the experimental results. **Figure 5** shows the appearance of the workpiece before and after deformation. As for the EBSD measurement results, **Fig. 6 -(a)** shows the inverse pole figure maps (color diagrams that show the crystal orientations on the observation plane)

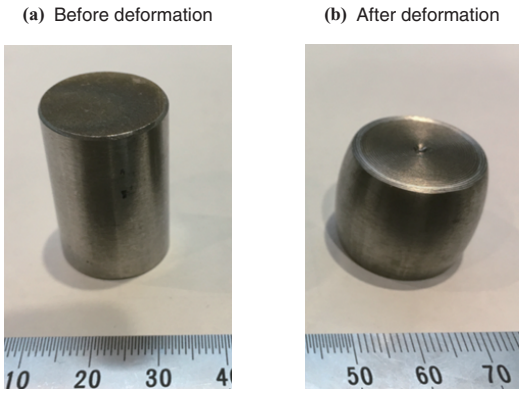

Fig. 5 Photographs of the workpiece

for each evaluation area before and after deformation. The black lines are grain boundaries (boundaries with a misorientation angle exceeding 5 degrees, except twin boundaries) as shown in **Fig. 6 -(b)**, and the colors seen in the crystal grains indicate the crystal orientations. Crystal grain shapes differ depending on their positions inside the workpiece, and their color variation trends differ slightly. Specifically, crystal grains with a shape that is flat in the workpiece's axial direction are observed here and there in the center part ① and the side part ②. This fact indicates that such crystal grains were distorted due to deformation. In addition, many crystal grains exhibit gradation in color inside them. This fact indicates that fine changes in crystal orientation occurred in each crystal grain due to deformation.

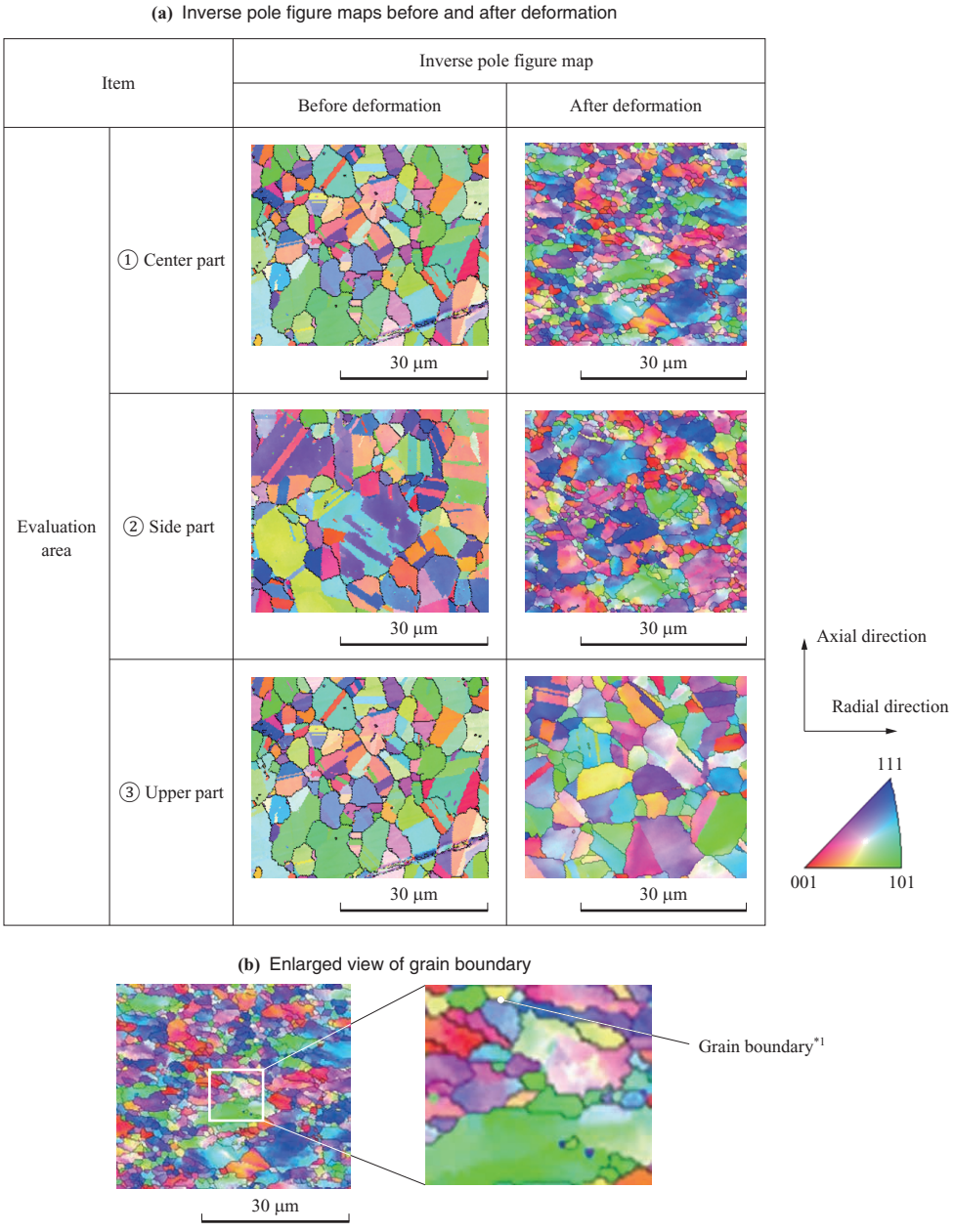

(Note) *1 : Boundaries with a misorientation angle exceeding 5 degrees, except twin boundaries

Fig. 6 Inverse pole figure maps obtained using EBSD data

By contrast, no marked differences from the state before deformation were observed in the upper part ③.

Figure 7 shows the pole figures (diagrams that show the crystal orientation distribution in the material with respect to the sample's coordinate system) before and after deformation. The numbers below the circles represent the crystal planes. In the pole figures, the distribution of points plotted in each circle represents the tendency in texture evolution throughout the entire measurement area. Before deformation, the points plotted in each evaluation area exhibited nearly the same random patterns. After deformation, by contrast, the plotted points exhibited distinctly different tendencies among the center part ①, the side part ②, and the upper part ③. In the center part ①, the distribution of the plotted points is clearly divided, which means the crystal orientations are directed nearly the same direction. Also, in the side part ②, the crystal orientations face a specific direction, however, the tendency is different from that of the center part ①. This difference in texture evolution tendencies is presumed to occur for the following reason: each evaluation area takes a different macroscopic strain state and accordingly differs in the direction in which the crystal orientations can easily rotate. In the upper part ③, by contrast, the distribution of the plotted points does not significantly change from the distribution observed before deformation, and the plotted points remain randomly distributed. This is because the upper part ③ is located in the dead metal region (a local region that is hardly deformed inside the material) around the workpiece's upper or lower end face.

4.2 Crystal plasticity FEM

Figure 8 shows the shape of the microscopic region at each evaluation area after deformation. The region corresponding to the center part ① has an isotropically expanded shape, which indicates that the region was simply compressed in the axial direction. The region corresponding to the side part ② has a shape indicating that the region was compressed in the axial direction as well as extended in the radial direction. The region corresponding to the upper part ③ (in a dead metal region) has a shape indicating that the region underwent almost no deformation. These results reflect the different strain states that were given as boundary conditions. Each element is distorted into a different shape. The initial crystal orientations and changes in crystal orientation during deformation differ depending on the integration point locations, and the deformation gradient is determined by the stress state and the crystal orientation. These factors caused the distortion. Therefore, each element is distorted in a different shape.

Figure 9 shows the pole figures observed before and after deformation. The texture evolution tendency differs depending on the evaluation area. This tendency is almost in

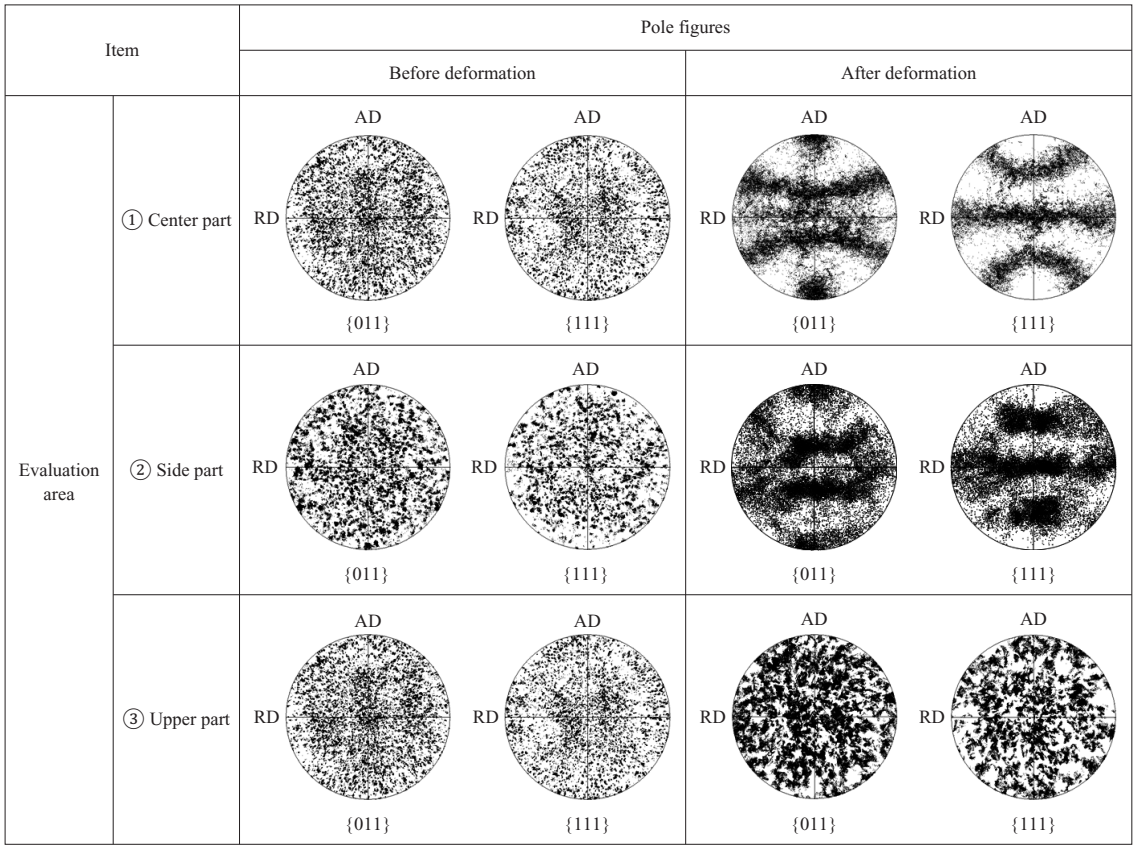

Fig. 7 Pole figures obtained using EBSD data

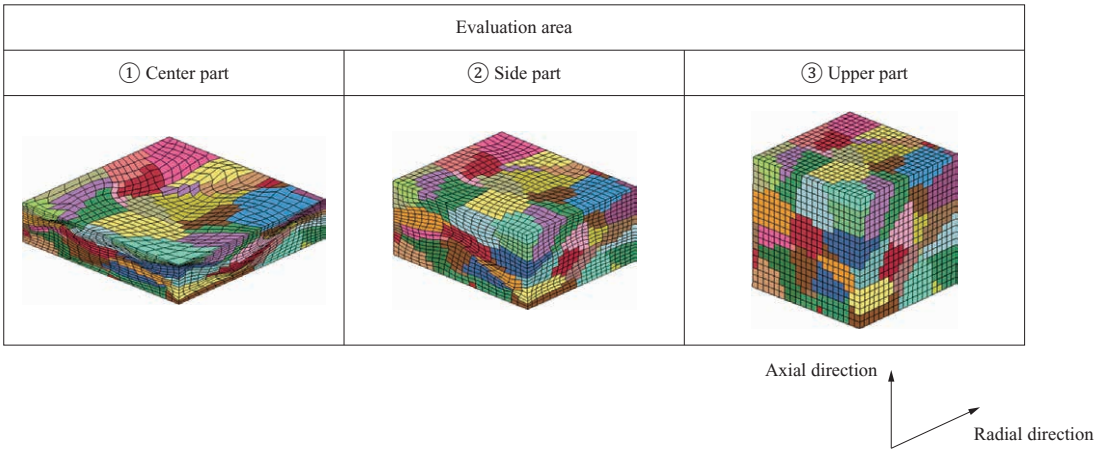

Fig. 8 Shapes of finite element models after compression simulated using the CP-FEM

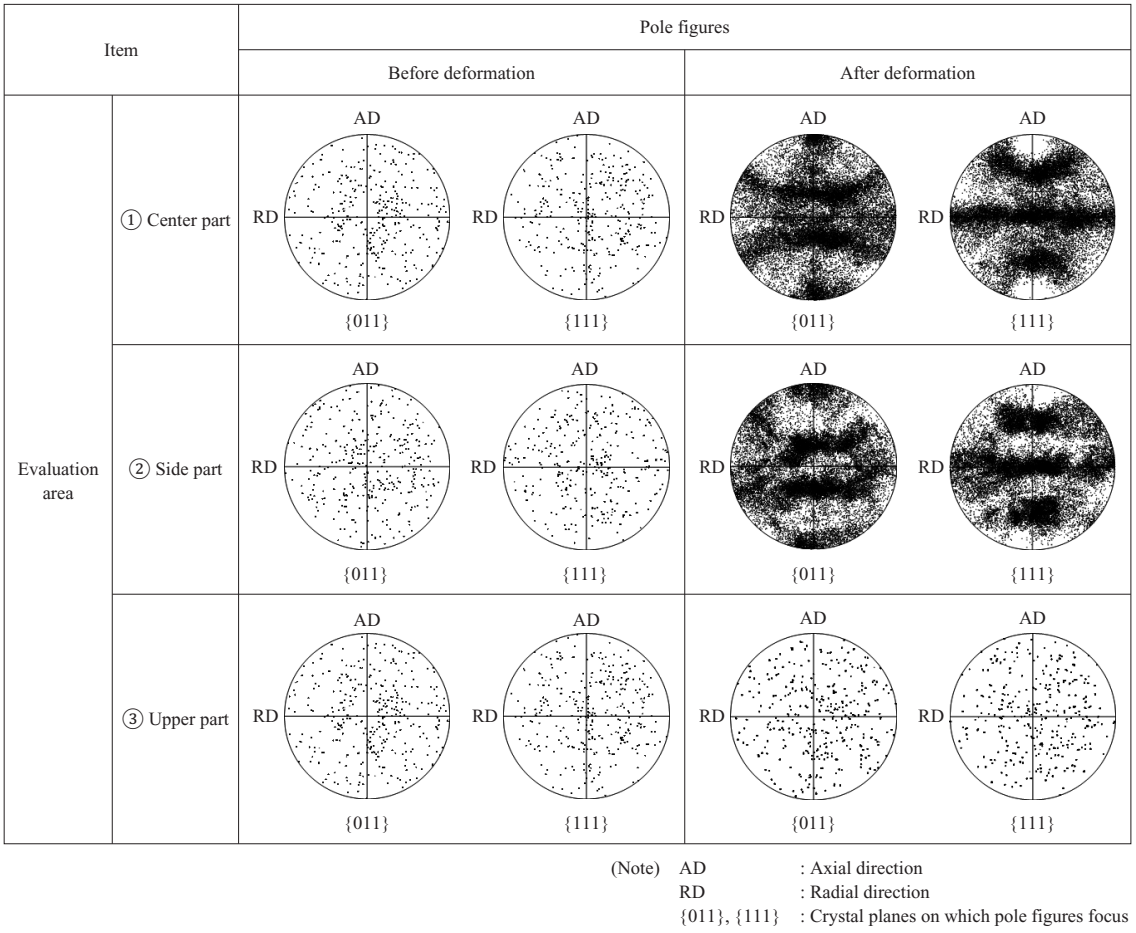

Fig. 9 Pole figures obtained using the CP-FEM

agreement with the EBSD measurement results shown in **Fig. 7**. This result indicates that the changes in crystal orientation that occur inside a material may be predict by performing crystal plasticity simulation on microscopic regions under boundary conditions established based on the results of ordinary rigid plasticity FEM.

In actual manufacturing processes, other microstructure evolutions (e.g., recrystallization, grain growth and phase transformation) may occur in addition to changes in crystal orientation due to deformation. To represent these phenomena, crystal plasticity FEM may be combined with another simulation method (e.g., the Cellular Automata method or Phase-Field method) to express microstructure evolution[5), (6)]. Our future work is to establish a framework of simulation techniques by applying such a combination of methods in order to predict grain size.

5. Conclusion

With the purposes of shortening the development period in process development and reducing the costs of trial

manufacture, we are engaged in the development of microstructure prediction techniques using simulation based on physically meaningful approaches. This paper described the possibility that changes in crystal orientation may be predicted by performing crystal plasticity simulation on the cold uniaxial compression deformation of Alloy718. To realize techniques for microstructure prediction in actual manufacturing processes, we will advance underlying techniques and establish a framework of simulation.

REFERENCES

(1) F. J. Humphreys and M. Hatherly : Recrystallization and Related Annealing Phenomena Second Edition, Elsevier, 2004

(2) M. Kuroda and K. Shizawa : Theory and application of crystal plasticity: From large deformation to dislocation accumulation, Journal of the Japan Society for Technology of Plasticity, Vol. 43, No. 495, 2002, pp. 33-43

(3) D. Peirce, R. J. Asaro and A. Needleman : Material rate dependence and localized deformation in crystalline solids, Acta Metallurgica, Vol. 31, Iss. 12, 1983, pp. 1 951-1 976

(4) H. Kuramae, Y. Ikeya, H. Sakamoto, H. Morimoto and E. Nakamachi : Multi-scale parallel finite element analyses of LDH sheet formability tests based on crystallographic homogenization method, International Journal of Mechanical Sciences, Vol. 52, Iss. 2, 2010, pp. 183-197

(5) H. Li, Xinxin Sun and He Yang : A three-dimensional cellular automata-crystal plasticity finite element model for predicting the multiscale interaction among heterogeneous deformation, DRX microstructural evolution and mechanical responses in titanium alloys, International Journal of Plasticity, Vol. 87, 2016, pp. 154-180

(6) L. Chen, J. Chen, R. A. Lebensohn, Y. Z. Ji, T. W. Heo, S. Bhattacharyya, K. Chang, S. Mathaudhu, Z. K. Liu and L.-Q. Chen : An integrated fast Fourier transform-based phase-field and crystal plasticity approach to model recrystallization of three dimensional polycrystals, Computer methods in applied mechanics and engineering, Vol. 285, 2015, pp. 829-848